Chemical Engineering Journal 174 (2011) 281–288

Contents lists available at SciVerse ScienceDirect

Chemical Engineering Journal

journal homepage: www.elsevier.com/locate/cej

Structural analysis of naproxen-intercalated bentonite (Unye)

A. Tabak[a,*], N. Yilmaz[a], E. Eren[b], B. Caglar[c], B. Afsin[d], A. Sarihan[b]

[a] Department of Chemistry, Faculty of Arts and Sciences, Rize University, 53100 Rize, Turkey
[b] Department of Chemistry, Faculty of Arts and Sciences, Bilecik University, 11210 Bilecik, Turkey
[c] Department of Chemistry, Faculty of Arts and Sciences, Erzincan University, 24030 Erzincan, Turkey
[d] Department of Chemistry, Faculty of Arts and Sciences, Ondokuz Mayis University, 55139 Samsun, Turkey

ARTICLE INFO

Article history:
Received 6 May 2011
Received in revised form 3 September 2011
Accepted 7 September 2011

Keywords:
Naproxen
Unye-bentonite
XRD
FTIR
TG/DTA/DSC
Surface area

ABSTRACT

The difference in the basal spacing (8.79 Å) and a higher mass loss (6.2%) in the temperature range of 200–750 °C of naproxen-bentonite (N-bentonite) comparing to that of Unye bentonite (UB) signified the existence of thermally stable organic species in the interlamellar space of the bentonite clay. The asymmetric OCO^- stretching band (1607 cm^{-1}) of N-bentonite became stronger in the temperature interval of 100–400 °C as a result of binding via the C=O group of the ligand to exchangeable cation and/or water molecule whereas the OH bending peak of water (1633 cm^{-1}) and the C=C stretching vibration of aromatic ring (1531 cm^{-1}) became weaker on thermal treatment. The effect of ionic strength on the desorption of naproxen species and the related kinetic data revealed that the release mechanism at pH = 7.4 is unrestricted diffusion controlled and governed by the repulsive interactions between the bentonite surface and the negatively charged species. The pore structure characteristics of the bentonite samples corresponding to the surface area, pore volume and pore size were determined by using the conventional analysis of the nitrogen adsorption–desorption isotherms.

1. Introduction

Natural clay minerals and modified clays such as organo-clays prepared by acid activation, ion-exchange, and pillaring are widely used as excipients and active agents in drugs [1,2]. Therefore, the surface properties of these materials referring to their roles in adsorption (desiccation or removal of water from the gas phase), purification of gas or liquid streams and bulk separation of a wide range of organic chemicals and catalytic processes (as catalysts of alkylation, dimerisation and cracking reactions for hydrocarbons) has been of interest [3,4]. The elucidation of the structural (specific surface area, sorption capacity, rheological properties) and compositional (chemical inertness and low or null toxicity for the patient) features of clays and clay minerals for medicinal purposes provided significant advantages in practical applications [5–7]. A comprehensive review of the utility of these materials in pharmaceutical formulations (gastrointestinal protectors, osmotic oral laxatives, antidiarrhoeaics, dermatological protectors and cosmetics), spas (geotherapy, pelotherapy and paramuds) and aesthetic medicine (to clean and moisturise the skin and to combat compact lipodystrophies, acne and cellulite) has been given by Carretero [8].

The beneficial effects of a drug for human health are closely related to targeting selected body parts at a desired concentration level of drug for prolonged period of time. This concentration level for therapeutic applications can be achieved without reaching a higher toxic level or dropping below the minimum effective level [9]. Natural clays and clay minerals may play a crucial role in modulating controlled delivery systems and, they can release the active substance at the desired biological site of the body in controlled manners [10,11]. This mechanism covers the penetration of drug into the interlayer space of the lamellar host and the release of it via diffusion and de-intercalation process [12]. Clay–drug interactions include the binding mechanisms of ionic, ion–dipole, hydrogen bonding, and van der Waals and, in some cases, covalent bonding is encountered depending on the molecular size, the type of the functional groups and physical–chemical properties of organic compounds inserted into the interlayer space of the clay as cationic or neutral species as well as the clay type [10,13]. The drug–clay complexes can be examined based upon the changes in the basal spacing, thermal stability, specific surface area and the pore size distribution [14,15]. Therefore, X-ray diffraction, thermal, Fourier Transform Infrared, and surface area analysis techniques which give invaluable information about the type of clay–organic interactions are of prime importance in characterizing the structures of these materials.

Bentonite clay, mainly composed of montmorillonite, consists of sheets of alumina octahedra and silica tetrahedra shared in a

* Corresponding author. Tel.: +90 4642236126; fax: +90 4642235376.
E-mail address: ahmtabak@hotmail.com (A. Tabak).

1385-8947/$ – see front matter © 2011 Elsevier B.V. All rights reserved.
doi:10.1016/j.cej.2011.09.027

2:1 ratio. The isomorphous replacement of a trivalent aluminium ion for a tetravalent silicon ion in the tetrahedral layer and a divalent magnesium or iron ion for a trivalent aluminium ion in the octahedral layer results in an excess charge which is balanced by the exchangeable cations such as Na^+, K^+, H^+, Ca^{2+}, etc., on the layer surfaces. The parallel layers in these structures which are held together by rather weak forces of van der Waals and electrostatic interactions are expandable by anchoring organic species and water molecules into the gallery spacing of clay [16,17]. Bentonite clay, having the releasing ability of these species in controlled sense, is suggested to be a good delivery carrier of various drugs because as the excipient, it plays an important role in dispersing active principles due to its ability to increase in volume in the presence of water, in buffering abrupt change of acidity, and in stabilizing emulsion, polar gel and suspension because of its colloidal characteristic to avoid the segregation of the pharmaceutical formulation's components [18–20].

Naproxen, systematic (IUPAC) name (+)-(S)-2-(6-methoxynaphthalene-2-yl) propanoic, is a non-steroidal anti-inflammatory drug commonly used for the reduction of moderate to severe pain, fever, inflammation and stiffness caused by conditions such as osteoarthritis, rheumatoid arthritis, psoriatic arthritis, gout, ankylosing spondylitis, menstrual cramps, tendonitis, bursitis, and the treatment of primary dysmenorrhea [21]. However, naproxen preparations containing sodium are not recommended for use in patients with sodium-sensitive hypertension, due to potential adverse effects on blood pressure.

In the present work, the thermal stability and structural properties of naproxen-bentonite (N-bentonite) composite prepared by treatment of naproxen with Unye bentonite (UB), which is an important clay mineral resource in Turkey, were investigated using X-ray diffraction (XRD), thermal analysis (TG/DTA/DSC), Fourier Transform Infrared (FTIR), and specific surface area measurement (BET) techniques by giving special emphasis to the nature of the interaction between naproxen and the clay.

2. Materials and methods

2.1. Materials

$CaCl_2{\cdot}6H_2O$ (Merck, 99.0%), $ZnCl_2$ (Merck, 99.0%), and (+)-(S)-2-(6-methoxynaphthalene-2-yl) propanoic (naproxen) were used for preparing the cation-exchanged- and naproxen-bentonite samples, respectively.

2.2. Preparation of Ca- and Zn-bentonite samples

5 g of raw-bentonite sample from Ordu/Unye region of Turkey was washed with deionized water several times and dried at 105 °C and then centrifuged at 6000 rpm. The bentonite sample was homoionized by treating with 100 ml of 0.1 M $CaCl_2$ solution. The Ca-bentonite product thus obtained was dried at 105 °C and sieved to 38–108 μm. The cation exchange capacity (CEC) value of UB, which is mainly Ca-montmorillonite, was determined as 74 mequiv/100 g clay by methylene blue adsorption technique and the chemical composition of the clay sample is given in Table 1 [22,23].

The Ca-bentonite sample was treated with 100 ml of 0.1 M $ZnCl_2$ solution at room temperature for 24 h under vigorous stirring. The product was washed with deionized water thoroughly and the supernatant was filtered off and the solid part was washed with deionized water repeatedly until a negative chloride test was attained. The solid precipitate was ground to the initial size and kept for spectroscopic measurements. In this study, the Zn cation selected for the cation exchange compared to the other cations was perfectly interacted to form the complex compound with naproxen molecule. This result may be explained in terms of the effect of ion size and charge of exchangeable cation.

Table 1
Chemical composition of the Unye bentonite.

Constituents	Weight (%)
SiO_2	62.70
Al_2O_3	20.10
Fe_2O_3	2.16
Na_2O	0.27
K_2O	2.53
CaO	2.29
MgO	3.64

2.3. Synthesis of naproxen-bentonite (N-bentonite)

The suspension of 3.0% (by mass) of Zn-bentonite in deionized water (400 ml) was treated with naproxen sodium solution in an ethyl alcohol/water (1:5) mixture (10 g/100 ml) at pH = 6 and 60 °C for 24 h under a nitrogen atmosphere. The N-bentonite was separated from ethyl alcohol/water mixture by centrifugation and washed with deionized water thoroughly which is followed by freeze-drying and grinding to 38–108 μm.

2.4. Desorption procedure

The naproxen-loaded bentonite samples were immersed in 150 ml aliquots of 0.1 M sodium phosphate buffer containing different amounts of sodium chloride, pH = 7.4 (PBS), and incubated on a constant temperature shaking bed at 37 °C and 130 rpm. After specific intervals, 1 ml aliquot of samples were withdrawn and immediately replaced with the same amount of fresh medium. 5 ml of solution were withdrawn at fixed intervals, filtered with Millex HV Millipore (ϕ = 45 μm) filters and immediately replaced with an equal volume of the buffer solution, in order to keep a constant volume. The amount of naproxen delivered from the samples was monitored by the Unicam UV2 UV-VIS spectrophotometer at λ = 332 nm. The kinetic analysis of the release process was carried out by fitting the data to the Korsmeyer–Peppas model [24–26]. The adsorption kinetics experiments were repeated in triplicate and the average values were reported.

2.5. Characterization of the bentonite samples

EDXRF spectrometer (Epsilon5, PANalytical) was used for chemical analysis of UB (Table 1). FTIR spectra of the raw and N-bentonite samples were recorded in the region of 4000–450 cm^{-1} on a Spectrum-100 FTIR spectrometer at a resolution of 4 cm^{-1}. XRD patterns were taken on a Rigaku 2000 automated diffractometer using Ni filtered CuKα radiation (λ = 1.54050 Å; 40 kV and 40 mA). Bragg's law, defined as $n\lambda = 2d\sin\theta$, was used to compute the crystallographic spacing (d) for the examined bentonite samples. The TG and DTA curves were scanned using a PYRIS Diamond TG/DTG apparatus in a dynamic nitrogen atmosphere (heating rate: 10 °C/min, platinum crucibles, mass ~10 mg and temperature range: 30–1000 °C). The DSC curves were collected on a PYRIS Diamond DSC apparatus in a static air atmosphere (heating rate: 10 °C/min, platinum crucibles, mass ~10 mg and temperature range: 30–750 °C).

Nitrogen adsorption/desorption isotherms were obtained in the relative pressure range of $0.05 < P/P_0 < 1.00$ using 0.2–0.5 g of sample with a Micromeritics ASAP 2020 V3.04 H analyzer. The samples were degassed at 150 °C for 6 h prior to the textural measurements at 77 K (−196 °C). Specific surface areas were determined from adsorption isotherms by applying the BET and Langmuir equations (S^{BET} and S^{L}, respectively). Mesoporous surface areas ($_{BJH}S^{mp}$) and

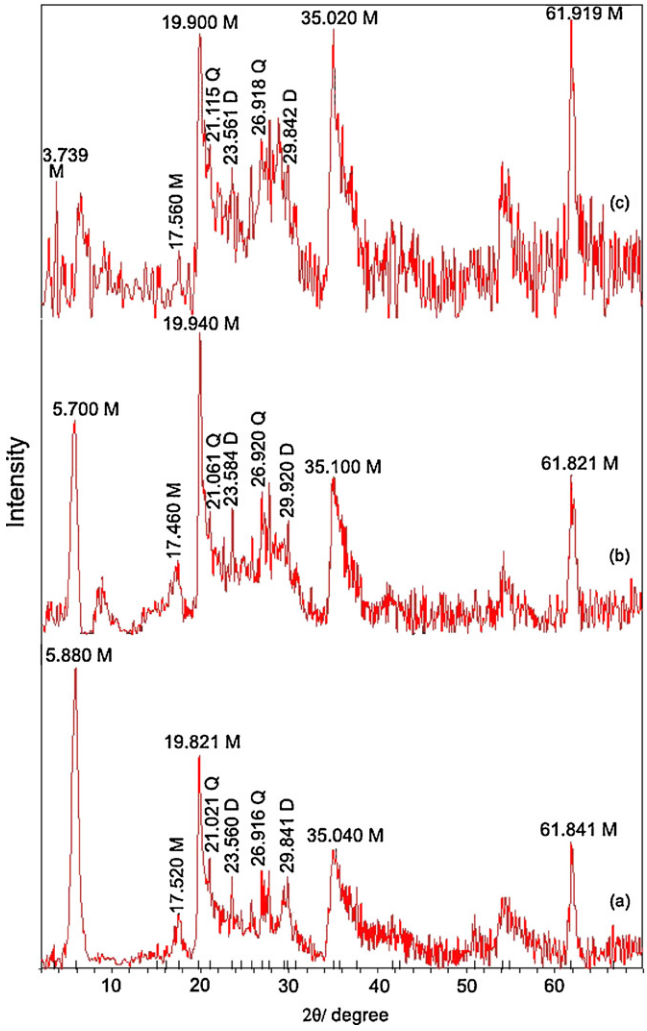

Fig. 1. The XRD spectra of (a) raw-bentonite, (b) Zn-bentonite, and (c) N-bentonite.

volumes ($_{BJH}V^{mp}$) were determined using the BJH method. Pore sizes were represented by both adsorption average pore width (4V/A by BET) and BJH adsorption average pore width (4V/A) (APWBET and APWBJH, respectively). S^{sp} is single point surface area.

3. Results and discussion

3.1. XRD data of raw, Zn- and N-bentonites

The XRD pattern of raw-bentonite is given in Fig. 1a. The d_{001}, d_{003}, $d_{020-110}$, $d_{130-200}$ and d_{060} diffractions corresponding to the main montmorillonite (M) component (80%) are seen at 5.880°, 17.520°, 19.821°, 35.040° and 61.841° (2θ) with the distances of 15.02, 5.06, 4.47, 2.56 and 1.50 Å, respectively. The bands originating from external clay components quartz (Q) and dolomite (D) are observed at 21.021° and 26.916° (2θ) with the distances of 4.22 and 3.31 Å and, at 23.560° and 29.841° (2θ) with the distances of 3.77 and 2.99 Å, respectively. The comparison of the peak intensity of the d_{001} peak of montmorillonite with the intensities of the peaks of the external clay components showed that the amounts of the quartz and dolomite impurities are not high. Significant amounts of Mg and Ca determined from the elemental analysis of the bentonite sample proved the existence of dolomite component as well as the framework Mg and interlayer Ca cations. The d_{001} distance of bentonite which is found to be higher than that of the d_{001} value of Na-montmorillonite (12.04 Å) may be explained by the presence of the interlayer Ca^{2+} and K^+ cations. The basal spacing of bentonite falling in the range of 14.45–15.40 Å indicates that the bentonite is a calcium-rich sample [27].

The d_{060} diffraction peak is taken into account as an important feature in determining the type of smectites. This peak is located in the range of 1.499–1505 Å for Al-rich dioctahedral 2:1 clay minerals (montmorillonite, beidellite, Al-rich mica, etc.) whereas it is seen at 1.549 Å for trioctahedral Mg-rich chlorite and it falls in the range of 1.55–1.56 Å for trioctahedral Fe-rich chlorite and bertherine [28]. The d_{060} peak was seen at 1.50 Å for raw-bentonite revealing that the sample used in the present study is an Al-rich dioctahedral montmorillonite.

The XRD pattern of Zn-bentonite is illustrated in Fig. 1b. The d_{001} peak of Zn-bentonite is observed at 5.70° (2θ) with a distance of 15.49 Å. The other diffraction peaks of bentonite are seen at 17.460°, 19.940°, 35.100° and 61.821° (2θ) and the diffraction peaks of quartz and dolomite are located at 21.061°, 26.920° (2θ) and 23.584°, 29.920° (2θ), respectively. Cation exchange processes occurring within the interlayer spacing of bentonite caused the changes and differences both in the position and the intensity of the main (0 0 1) peak. The intensity variation of the main peak affected the relative intensities of the other diffraction peaks as well as those of the external clay components depending on the amount of the cation exchange. However, there seemed no relation between the radii of the inserted cations and the observed d_{001} distances. Therefore, this situation may be connected with the ratio of the amount of the cation inserted and coordinated water and, the electrostatic attraction between the cations and the interlayer surface planes [23]. Furthermore, a few studies pointed out that the exchangeable cation in the clay catalyst which was determined by the standard methods after extracting with dilute hydrochloric acid showed that the amount of cation exchange was almost equivalent to CEC [29,30].

The d_{001} basal spacing value of the N-bentonite is determined as 23.61 Å at 3.739° (2θ) (Fig. 1c). The expansion by 2.14° (2θ) or 8.59 Å of the d_{001} spacing of the bentonite on the formation of N-bentonite confirmed that naproxen molecules were inserted in between the bentonite layers by replacing the interlayer water molecules. An interlayer opening caused by this insertion process was estimated to be 14.61 Å by subtracting the thickness of SiO_2–Al_2O_3–SiO_2 sheet (9.0 Å) from the d(0 0 1) value of N-bentonite. Keying of naproxen molecule into the interlayer increased the d(0 0 1) value by about 14.61 Å along the c axis which is below the expected basal spacing of bentonite [31]. Finally, it may be suggested from the d_{001} value of N-bentonite and the length of naproxen molecule (12.20 Å) that the organic species might be oriented as a partially superimposed monolayer in the interlamellar spacing [32].

3.2. Thermal analysis data of raw, Zn- and N-bentonites

The dehydration process of clay minerals which occurs at low temperatures is followed by the dehydroxylation at intermediate temperatures and the phase transition taking place at relatively high temperatures [33]. External clay components and impurities may also be exposed to thermal decomposition. The thermal analysis data of raw-bentonite are shown in Fig. 2a and Table 2. On the TG curve of raw-bentonite, two dehydration stages with a total mass loss of 10.7% in the range of 30–200 °C are noticeable. In the first stage, the removal of adsorbed water in the region of 30–120 °C gives rise to an endothermic peak maximum of 76 °C on the DTA curve. The DTA endotherm at 141 °C which is accompanied by a mass loss of 2.2% is ascribed to the elimination of the water species coordinated to the interlayer cations. In addition, the mass losses by 1.1 and 2.8% in the temperature ranges of 200–500 and 500–750 °C

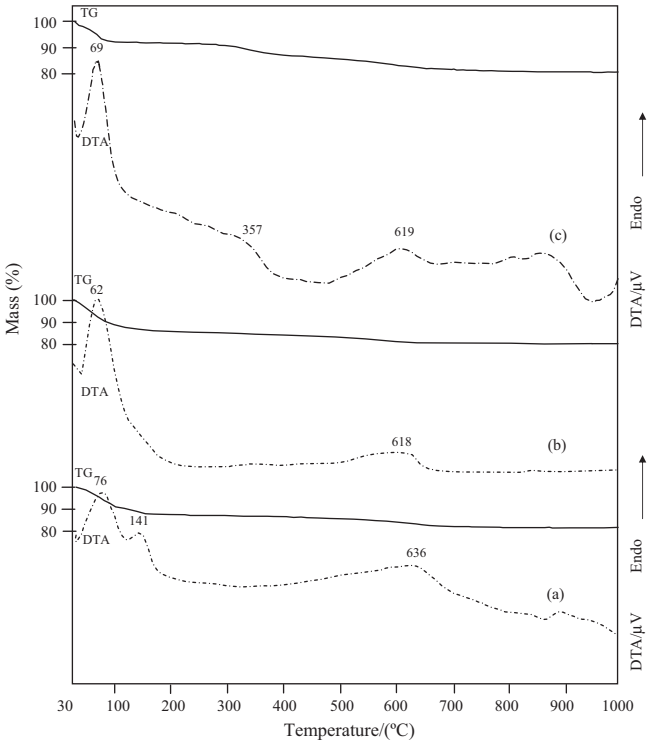

Fig. 2. Thermal analysis curves of (a) raw-bentonite, (b) Zn-bentonite, and (c) N-bentonite.

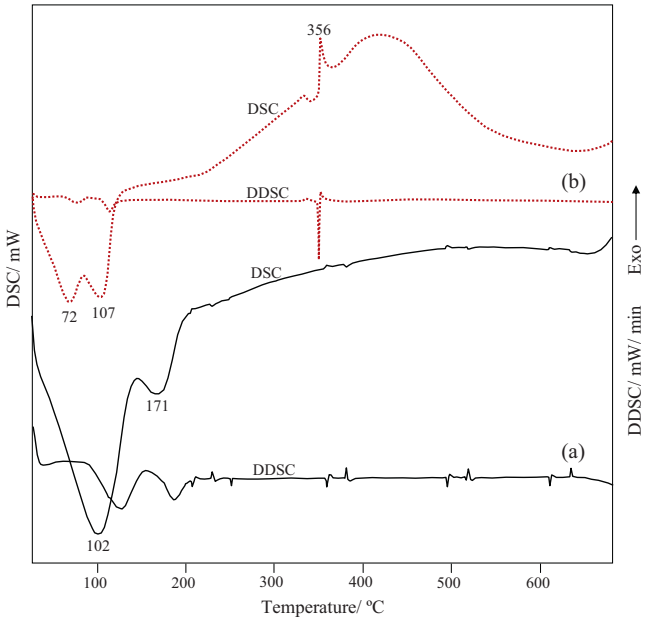

Fig. 3. DSC–DDSC curves of (a) raw-bentonite and (b) N-bentonite.

on the TG curve, respectively, represent the removal of external clay components and structural OH groups, respectively.

Thermal analysis results of Zn-bentonite (Fig. 2b and Table 2) are similar to those of raw-bentonite. The mass losses by 11.4 and 4.2% in the temperature ranges of 30–200 and 200–750 °C, respectively, point out the evolution of interlayer water and dehydroxylation of lattice water which is accompanied by the decomposition of external clay components, respectively.

In the case of N-bentonite, the endothermic DTA peaks are attributed to the removal of interlayer organic species with a continuous mass loss of 10.2% in the temperature range of 200–750 °C (Fig. 2c). The exothermic peak at 356 °C with a decomposition enthalpy of −0.54 mJ mg^{-1} on the DSC curve of N-bentonite (Fig. 3b and Table 2) corroborates this result. In addition, the decrease in total water amount (7.1%) removed from N-bentonite in the range of 30–200 °C in comparison with the raw-bentonite and Zn-bentonite samples may be explained by the replacement of outer sphere water entities by naproxen species [34,35]. The water types of lower decomposition energy on the DSC curve of N-bentonite comparing to that of raw-bentonite in the same temperature range may be taken as another evidence confirming this result (Fig. 3a and b and Table 2). Furthermore, the higher total mass loss of N-bentonite than the raw and Zn-bentonites in the temperature range of 200–750 °C illustrates the gradual decomposition of the organic molecule and the release of high amounts of organic H_2O and CO_2 species are released (Table 2) as a result of high-temperature oxidation of black residue [36]. The thermal stability of the interlamellar organic species up to 750 °C also signifies the presence of π interactions between the oxygen planes of the clay sheet and aromatic ring of the molecule, and the shielding effect of alumino-silicate layers [16,37,38].

3.3. IR spectral data of raw, Zn- and N-bentonites

The IR spectrum of the raw-bentonite is given in Fig. 4a. The structural OH stretching vibrations appear in the range of 3700–3200 cm^{-1}, the Si–O stretching vibration and the OH bending modes are seen in the range of 1300–440 cm^{-1} [39,40]. The peak at 3620 cm^{-1} originates from the Al_2OH stretching. The broad peak at 3434 cm^{-1} which belongs to the OH stretching of H-bonded water of raw-bentonite is intensified because of the higher amount of octahedral replacement of Mg atoms than that of Fe atoms [40–43]. The peaks originating from the external clay components such as quartz and dolomite are located at 790 and 698 cm^{-1}, respectively. The peak at 1638 cm^{-1} belongs to the OH deformational

Table 2
Thermal analysis data of raw-bentonite, Zn-bentonite and N-bentonite.

Sample	DSC_{max} (°C)	ΔH (mJ mg^{-1})	DTA_{max} (°C)	Temperature range (°C)	Mass loss (%)	Total mass loss (%)
Raw-bentonite	102	47.7	76	30–120	8.54	
	171	7.05	141	120–200	2.18	
	–	–	–	200–500	1.14	
	–	–	636	500–750	2.85	14.71
Zn-bentonite	–	–	62	30–120	10.00	
	–	–	–	120–200	1.40	
	–	–	–	200–500	1.57	
	–	–	618	500–750	2.60	15.57
N-bentonite	72	3.96	69	30–120	7.50	
	107	8.34	–	120–200	0.45	
	356	−0.54	357	200–500	5.69	
	–	–	619	500–750	4.55	18.19

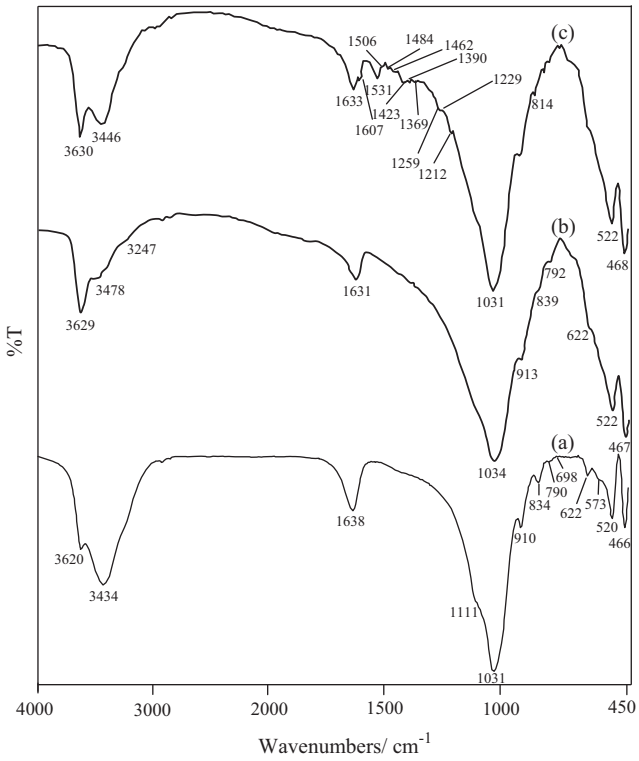

Fig. 4. The FTIR spectra of (a) raw-bentonite, (b) Zn-bentonite, and (c) N-bentonite.

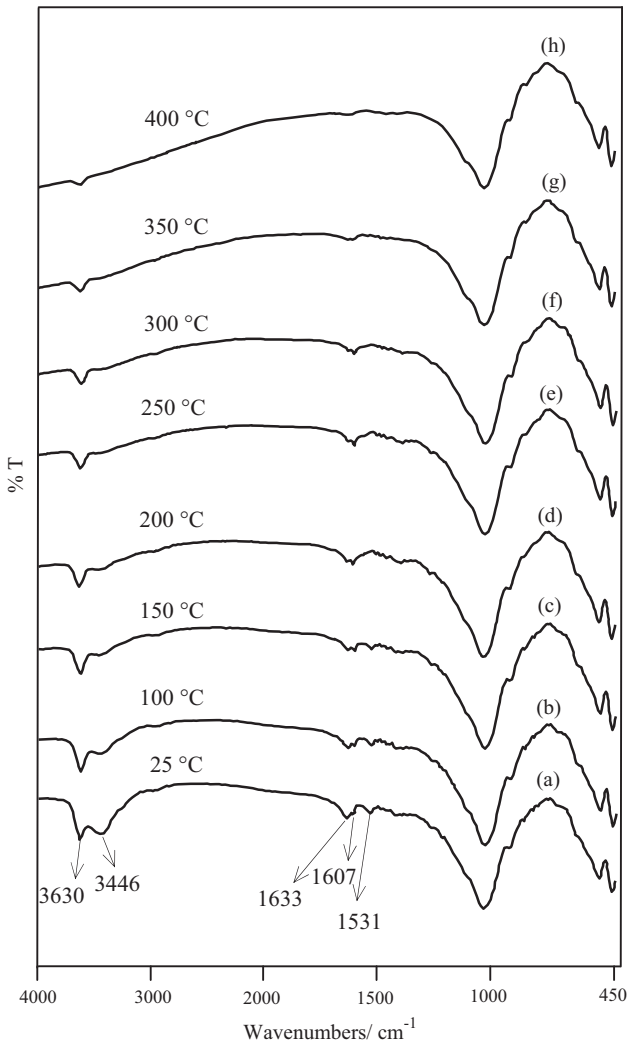

Fig. 5. FTIR spectra of N-bentonites (a–h) heated in the interval temperature of 25–400 °C, respectively.

mode of water and the peak at 1111 cm^{-1} is the longitudinal Si–O stretching mode. The Si–O–Si and Al–O–Si stretching peaks of tetrahedral layer was clearly seen at 1031 and 520 cm^{-1}, respectively. The OH bending peaks of octahedral layer was observed at 910 and 834 cm^{-1}. The Al_2OH and AlMgOH bending peaks point out the octahedral substitution process. Based on the peaks of raw-bentonite, it may be concluded that the Al atoms predominate the centers of octahedral layer and the amount of Mg atoms is significant. Both the XRD patterns and the vibrational features prove that the raw-bentonite sample consists of an Al-rich dioctahedral montmorillonite component.

The IR spectrum of Zn-bentonite is shown in Fig. 4b. In general, the exchange process between the new and exchangeable cations did not exhibit significant differences in the IR spectrum of the raw-bentonite. However, it is possible to come across to some distinctions in the OH vibrational peaks due to the differences of the binding abilities of the metal cations towards the interlayer water species since the water molecule is preferably coordinated to the interlayer cations and the residual water is retained by the interlayer holes. The water molecules coordinating to the cations can emigrate to the bi-trigonal cornered holes on siloxane surface affecting the OH groups and thus, change the intensities of the corresponding peaks [23,42,44]. In the IR spectrum of Zn-bentonite, the OH-groups involved in H_2O–H_2O H-bonds give rise to the vibrations around 3478 cm^{-1}, and the small shoulder at 3247 cm^{-1} may be ascribed to an overtone of the H_2O bending vibration. Because of the polarizing power of the Zn^{2+} cations, stronger H-bonds to water species are expected to form in outer coordination spheres, and thus, the band at 3247 cm^{-1} which is probably due to the M^{2+}–OH vibration is intensified [42,45].

The (C=C) aromatic ring and the deformation vibrations of alkyl groups in the ranges of 1600–1430 and 1480–1360 cm^{-1}, respectively, are clearly seen in the IR spectrum of N-bentonite shown in Fig. 4c. The C–H in plane bending peaks of alkyl groups are located at 1484, 1462, 1451, 1369 and 1363 cm^{-1}, the C–O stretching of carboxyl at 1212 and 1229 cm^{-1}, the O–H in plane bending at 1412 and 1423 cm^{-1}, the C–O stretching of aromatic ring's ether at 1259 cm^{-1} and, the vibrations of aromatic ring (C=C) at 1531 and 1506 cm^{-1} all demonstrate that the naproxen entities are penetrated into the interlamellar space of bentonite. The asymmetric and symmetric OCO^- stretching peaks of carboxylate species emerging at 1607 and 1390 cm^{-1}, respectively, may be taken as another evidence to the penetration process. It may be concluded from the positional difference by $\Delta\nu = 217\ cm^{-1}$ between the asymmetric and symmetric OCO^- stretching bands that the naproxen molecule is most likely bound to the interlayer metallic cation of bentonite through bidentate or bridging form [46–56].

The thermo-IR-spectra were recorded in the range from room temperature to 400 °C to follow the decomposition process of the N-bentonite complex (Fig. 5a–h). The dehydration and decomposition of N-bentonite at 200 °C resulted in the weakening of the OH bending mode of water (1633 cm^{-1}) and the C=C stretching vibration of aromatic ring (1531 cm^{-1}) in addition to the intensification of the asymmetric OCO^- stretching peak at 1607 cm^{-1} (Fig. 5d). These intensity changes became more significant as the decomposition of N-bentonite progressed at higher temperatures, with the substantial mass loss happening over 350 °C. The strengthening of the asymmetric OCO^- stretching band in parallel with the temperature increase may be related to the binding of the molecule

Table 3
Structure parameters of raw-bentonite, Zn-bentonite and N-bentonite.

Sample	Raw-bentonite	Zn-bentonite	N-bentonite
S^{BET} ($m^2\ g^{-1}$)	71.83	47.67	4.39
S^{L} ($m^2\ g^{-1}$)	97.18	65.01	6.27
S^{sp} ($m^2\ g^{-1}$)	71.63	46.95	4.33
${}_{BJH}S^{mp}$ ($m^2\ g^{-1}$)	29.35	24.23	3.41
${}_{BJH}V^{mp}$ ($cm^3\ g^{-1}$)	0.093	0.080	0.034
APWBET (nm)	5.82	6.82	25.62
APWBJH (nm)	12.71	13.26	39.36

through the C=O group of the ligand to exchangeable cation and/or water molecule. This mechanism also confirms two possible binding geometries (bridging and bidentate type) between the ligand and metallic cation.

3.4. Surface area measurements of raw-, Zn- and N-bentonites

Clay minerals are of aluminosilicate structures and their surface areas are related to the numbers and dimensions of internal and external pores they contain [45,57–59]. The total number of micropores and mesopores has a primer importance on the surface areas and adsorption properties of clays but the contribution of macropores to these characteristics is of negligible level. The textural parameters of raw, Zn-bentonite and N-bentonite samples were given in Table 3. The higher specific surface area of the raw-bentonite (71.83 $m^2\ g^{-1}$) comparing to the Zn-bentonite (47.67 $m^2\ g^{-1}$) signified that the pore opening effect is the dominant factor in the increase of the BET surface area [60]. In the interlayer space of the bentonite, the increase in the amount of the water species coordinated to Zn^{2+} cation (ionic size ≅ 0.80 Å) than the exchangeable Ca^{2+} cation (ionic size ≅ 1.06 Å) may induce structural expansion and the larger pore space [16,61]. The increase in the mesoporous surface area/the specific surface area ratio (~0.51) and the bigger average pore width (13.26 nm) of Zn-bentonite with respect to those of the raw-bentonite (~0.41 and 12.71 nm, respectively) may be taken as other proofs to these results (Table 3). These results also confirmed that the zinc ions were introduced inside the clay interlayer not only by cation exchange at planar sites, but also through the interaction with the aluminosilicate sheets [62]. In addition, the specific surface area of raw-bentonite (71.83 $m^2\ g^{-1}$) decreased by ca. 16-fold for N-bentonite (4.39 $m^2\ g^{-1}$), while the mesoporous volume (0.093 $cm^3\ g^{-1}$) decreased the value of 0.034 $cm^3\ g^{-1}$ (Table 3). The decrease in the surface area of N-bentonite may be explained in terms of the pore openings blocked (pore blocking effect) by the larger naproxen species which possess a closer packing in the interlamellar space [16,63,64]. On the other hand, because of the capillary condensation in the macropore range, the bigger mean pore size of N-bentonite (39.36 nm) in comparison with raw-bentonite (12.71 nm) can be ascibed to the increase in the number of mesopores and macropores, and the change in the porosity distribution [64].

3.5. Release behavior of N-bentonite

The ionic strength of the solution is one of the factors that controls both electrostatic and non-electrostatic interactions between the adsorbate and the adsorbent surface [65,66]. Fig. 6 shows the desorption isotherms of naproxen from the N-bentonite sample at different NaCl concentrations in the range of 0.2–1.0 mol/L at pH = 7.4. The increase in the ionic strength of the solution caused an increase in the desorption of naproxen from the bentonite surface. Under the screening effect of the added salt, the bentonite surface became negatively charged which induced the repulsive forces between the naproxen anion and the clay surface [67,68], suggesting that the desorption of naproxen is mainly governed by

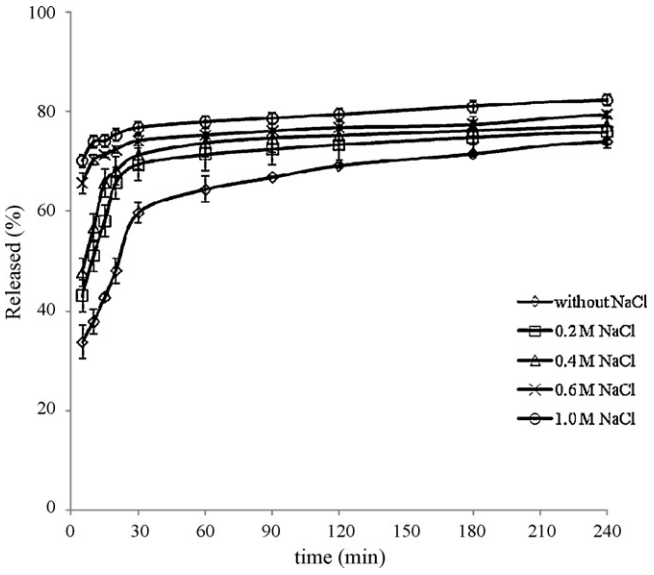

Fig. 6. The release profiles of naproxen at different electrolyte concentrations and pH = 7.4.

electrostatic interaction at pH = 7.4. The repulsive forces of the bentonite are very weak because of its zero point of charge (pH_{PZC}) very close to that of the solution pH (6.8 versus 7.4) [69]. Therefore, this observation can be relevant to the competition between the naproxen species for the adsorption sites on the bentonite surface in parallel with the Na^+ concentration.

In order to gain information about the release mechanism of naproxen, we have applied the Korsmeyer–Peppas model [25], which is a generalized formula arising from the Higuchi equation [70]:

$$\frac{M_t}{M_\infty} = kt^n,$$

where M_t and M_∞ correspond to the amount of drug released at a given time t and at infinite time, respectively; k is the rate constant related to structural parameters of the system and n is the release exponent which gives information about the kinetics of drug delivery. This mathematical model is linear for values of M_t/M_∞ lower than 0.6 and if n is 0.5 it means that a Fickian-transport mechanism is valid (Higuchi model), but if n values is ranged between 0.5 and 1.0 the release follows an anomalous mechanism. The kinetic data obtained for the systems here studied are summarised in Table 4. It may be suggested referring to some drug release studies that the clearly faster release of naproxen species from the N-bentonite composite might be interpreted in terms of the unrestricted diffusion of the naproxen to the dissolution medium due to the high accessibility [11,12,71,72]. It is well known that as a short time approximation the Korsmeyer–Peppas model cannot be applied beyond the 60% release [73]. The restricted release of naproxen species in the interlayer space of the bentonite may be explained in terms of the presence of interactions between the oxygen planes of

Table 4
Kinetic parameters calculated for the ionic strength mediums according to the Korsmeyer–Peppas model.

Ionic strength	k (1/min)	n	R
Without NaCl	0.19	0.31	0.935
0.2 M NaCl	0.28	0.27	0.967
0.4 M NaCl	0.33	0.23	0.963
0.6 M NaCl	0.59	0.06	0.966
1.0 M NaCl	0.65	0.04	0.948

k, rate constant; n, the release exponent; R, correlation coefficient.

the clay sheets and the aromatic ring of the organic molecule, and shielding effect of alumino-silicate layers [37,38]. Consequently, the amount of drug release at pH = 7.4 did not reach 100%.

4. Conclusions

The structural properties of the naproxen-bentonite sample were investigated by means of X-ray diffraction (XRD), thermal analysis (TG, DTA and DSC), and Fourier Transform Infrared (FTIR) spectroscopic techniques. The data revealed that the organic compound penetrated into the interlayer spacing of the bentonite as the neutral molecule, displacing water species. The binding of the naproxen molecule via the C=O group to the exchangeable cations either through a water bridge or a direct linkage to the cation is proved by the presence of the prominent asymmetric OCO^- stretching band after thermal treatment. The difference between the positions of the asymmetric and symmetric OCO^- stretching bands seems also parallel with these bonding configurations. The higher stability of N-bentonite than raw-bentonite in the temperature range of 200–700 °C signified the binding strength between the naproxen molecules and the clay sheets. The decomposition energy values on DSC curve and the decrease in the surface area of N-bentonite also support these results. Furthermore, the amount of drug release at pH = 7.4 value increases in line with the ionic strength of the medium. This result is ascribed to the release mechanism governed by unrestricted diffusion controlled repulsive interaction between the negatively charge bentonite surface and the anionic naproxen species. The minimum surface area and maximum pore size for N-bentonite were achieved as a result of the pore openings blocked by the naproxen species.

References

[1] C.S.F. Gomes, J.B.P. Silva, Minerals and clay minerals in medical geology, Appl. Clay Sci. 36 (2007) 4–21.
[2] J.L. Legido, C. Medina, M.L. Mourelle, M.I. Carretero, M. Pozo, Comparative study of the cooling rates of bentonite, sepiolite and common clays for their use in pelotherapy, Appl. Clay Sci. 36 (2007) 148–160.
[3] R.S. Taylor, Molecular separators in industrial use present and future, in: I.V. Mitchell (Ed.), Pillared Layered Structures: Current Trends and Applications, Elsevier, London, 1990, pp. 3–12.
[4] L.H. Little, Infrared Spectra of Adsorbed Species, Academic Press, London, 1966, pp. 180–199.
[5] J.W. McGinity, M.R. Haris, Influence of a montmorillonite clay on the properties of griseofulvin tablets, Drug Dev. Ind. Pharm. 6 (1980) 49–59.
[6] C. Viseras, C. Aguzzi, P. Cerezo, A.L. Galindo, Uses of clay minerals in semisolid health care and therapeutic products, Appl. Clay Sci. 36 (2007) 37–50.
[7] J.H. Choy, S.J. Choi, J.M. Oh, T. Park, Clay minerals and layered double hydroxides for novel biological applications, Appl. Clay Sci. 36 (2007) 122–132.
[8] M.I. Carretero, Clay minerals and their beneficial effects upon human health, Appl. Clay Sci. 21 (2002) 155–163.
[9] D. Depan, A.P. Kumar, R.P. Singh, Cell proliferation and controlled drug release studies of nanohybrids based on chitosan-g-lactic acid and montmorillonite, Acta Biomater. 5 (2009) 93–100.
[10] C. Aguzzi, P. Cerezo, C. Viseras, C. Caramella, Use of clays as drug delivery systems: possibilities and limitations, Appl. Clay Sci. 36 (2007) 22–36.
[11] H. Jung, H.M. Kim, Y.B. Choy, S.J. Hwang, J.H. Choy, Itraconazole-laponite: kinetics and mechanism of drug release, Appl. Clay Sci. 40 (2008) 99–107.
[12] J.K. Park, Y.B. Choy, J.M. Oh, J.Y. Kim, S.J. Hwang, J.H. Choy, Controlled release of donepezil intercalated in smectite clays, Int. J. Pharm. 359 (2008) 198–204.
[13] N.C. Papin, S. Cai, J. Vatier, F. Keller, C.H. Souleau, R. Farinotti, Drug interactions with diosmectite: a study using the artificial stomach–duodenum model, Int. J. Pharm. 182 (1999) 111–119.
[14] G.V. Joshi, H.A. Patel, B.D. Kevadiya, H.C. Bajaj, Montmorillonite intercalated with vitamin B1 as drug carrier, Appl. Clay Sci. 45 (2009) 248–253.
[15] M.E. Parolo, M.C. Savini, J.M. Valles, M.T. Baschini, M.J. Avena, Tetracycline adsorption on montmorillonite: pH and ionic strength effects, Appl. Clay Sci. 40 (2008) 179–186.
[16] A. Tabak, B. Afsin, S.F. Aygun, E. Koksal, Structural characteristic of organo-modified bentonites of different origin, J. Therm. Anal. Calorim. 87 (2007) 375–381.
[17] A. Tabak, B. Afsin, B. Caglar, E. Koksal, Characterization and pillaring of a Turkish bentonite (Resadiye), J. Colloid Interface Sci. 313 (2007) 5–11.
[18] D.E. Wurster, P. Gerald, Polli, Investigation of drug release from solids. V. Simultaneous influence of adsorption and viscosity on the dissolution rate, J. Pharm. Sci. 53 (1964) 311–314.
[19] M.W. Scott, H.A. Lieberman, A.S. Rankell, J.V. Battista, Continuous production of tablet granulations in a fluidized bed. I. Theory and design considerations, J. Pharm. Sci. 53 (1964) 314–320.
[20] J.H. Choy, M. Park, Cationic and anionic clays for biological applications, in: K.G. Satyanarayana (Ed.), Clay Surfaces: Fundamentals and Applications, Academic Press, 2004, pp. 407–424.
[21] From Wikipedia, the free encyclopedia.
[22] G. Kahr, F.T. Madsen, Determination of the cation exchange capacity and the surface area of bentonite, illite and kaolinite by methylene blue adsorption, Appl. Clay Sci. 9 (1995) 327–336.
[23] B. Caglar, B. Afsin, A. Tabak, E. Eren, Characterization of the cation-exchanged bentonites by XRPD, ATR, DTA/TG analyses and BET measurement, Chem. Eng. J. 149 (2009) 242–248.
[24] P. Costa, J.M. Sousa Lobo, Modelling and comparison of dissolution profiles, Eur. J. Pharm. Sci. 13 (2001) 123–133.
[25] R.W. Korsmeyer, R. Gurny, E. Doelker, P. Buri, N.A. Peppas, Mechanisms of solute release from porous hydrophilic polymers, Int. J. Pharm. 15 (1983) 25–35.
[26] N.A. Peppas, Analysis of Fickian and non-Fickian drug release from polymers, Pharm. Acta Helv. 60 (1985) 110–111.
[27] M. Önal, Y. Sarıkaya, Preparation and characterization of acid-activated bentonite powders, Powder Technol. 172 (2007) 14–18.
[28] J. Srodon, V.A. Drits, D.K. McCarty, J.C.C. Hsıeh, D.D. Eberl, Quantitative X-ray diffraction analysis of clay-bearing rocks from random preparations, Clays Clay Miner. 49 (2001) 514–528.
[29] A.I. Vogel, Textbook of Quantitative Inorganic Analysis, ELBS & Longman, 1978.
[30] C.R. Reedy, G. Nagendrappa, B.S.J. Parakash, Surface acidity study of M^{n+}-montmorillonite clay catalysts by FT-IR spectroscopy: correlation with esterification activity, Catal. Commun. 8 (2007) 241–246.
[31] A. Yamagishi, Racemic adsorption of iron(II) tris(1,10-phenanthroline) chelate on a colloidal clay, J. Phys. Chem. 86 (1982) 2472–2479.
[32] M. Wei, S. Shi, J. Wang, Y. Li, X. Duan, Studies on the intercalation of naproxen into layered double hydroxide and its thermal decomposition by in situ FT-IR and in situ HT-XRD, J. Solid State Chem. 177 (2004) 2534–2541.
[33] R.W. Grimshaw, The Chemistry Physics of Clays, Ernest Benn Ltd., London, 1971, pp. 968–979.
[34] A. Tabak, B. Afsin, S.F. Aygun, H. Icbudak, Phenanthroline Cu(II)-bentonite composite characterization, J. Therm. Anal. Calorim. 81 (2005) 311–314.
[35] W. Xie, Z. Gao, K. Liu, W.P. Pan, R. Vaia, D. Hunter, A. Singh, Thermal characterization of organically modified montmorillonite, Thermochim. Acta 367 (2001) 339–350.
[36] S. Yariv, The role of charcoal on DTA curves of organo-clay complexes: an overview, Appl. Clay Sci. 24 (2004) 225–236.
[37] M. Bora, J.N. Ganguli, D.K. Dutta, Thermal and spectroscopic studies on the decomposition of [Ni{di(2-aminoethyl)amine}$_2$]- and [Ni(2,2′:6′,2″-terpyridine)$_2$]-montmorillonite intercalated composites, Thermochim. Acta 346 (2000) 169–175.
[38] Z. Yermiyahu, A. Landau, A. Zaban, I. Labides, S. Yariv, Monoionic montmorillonites treated with Congo-Red, J. Therm. Anal. Calorim. 72 (2003) 431–441.
[39] J. Madejova, J. Bujdak, M. Janek, P. Komadel, Comparative FT-IR study of structural modifications during acid treatment of dioctahedral smectites and hectorite, Spectrochim. Acta Part A 54 (1998) 1397–1406.
[40] J. Madejova, FTIR techniques in clay mineral studies, Vib. Spectrosc. 31 (2003) 1–10.
[41] V.C. Farmer, in: V.C. Farmer (Ed.), The Layered Silicates. In the Infrared Spectra of Minerals, The Mineralogical Society, London, 1974, pp. 331–359.
[42] W. Xu, C.T. Johnston, P. Parker, S.F. Agnew, Infrared study of water sorption on Na-, Li-, Ca-, and Mg-exchanged (SWy-1 and Saz-1) montmorillonite, Clays Clay Miner. 48 (2000) 120–131.
[43] J.T Kloprogge, R. Evans, L. Hickley, R.L. Frost, Characterisation and Al-pillaring of smectites from Miles, Queensland (Australia), Appl. Clay Sci. 20 (2002) 157–163.
[44] J. Madejova, M. Janek, P. Komadel, H.J. Herbert, H.C. Moog, FTIR analyses of water in MX-80 bentonite compacted from high salinary salt solution systems, Appl. Clay Sci. 20 (2002) 255–271.
[45] C.C. Wang, L.C. Juang, C.K. Lee, T.C. Hsu, J.F. Lee, H.P. Chao, Effect of exchanged surfactant cation on the pore structure and adsorption characteristics of montmorillonite, J. Colloid Interface Sci. 280 (2004) 27–35.
[46] H. Nakatsuji, M. Yoshimoto, Y. Umemura, S. Takagi, M. Hada, Theoretical study of the chemisorption and surface reaction of HCOOH on a ZnO (1 0 1 0) surfaces, J. Phys. Chem. 100 (1996) 694–700.
[47] A. Glisenti, Interaction of formic acid with Fe_2O_3 powder under different atmospheres: an XPS and FTIR study, J. Chem. Soc., Faraday Trans. 94 (1998) 3671–3676.
[48] B. Afsin, M. Gökdere, N. Tınkılıç, Stability of hydroxy-formate species at a Pb(1 1 0) surface, Spectrochim. Acta Part B 55 (2000) 985–990.
[49] F. Kooli, T. Sasaki, F. Mizukami, M. Watanabe, C. Martin, V. Rives, Characterization and acidic properties of silica pillared titanates, J. Mater. Chem. 11 (2001) 841–845.
[50] G.C. Cabilla, A.L. Bonivardi, M.A. Baltanas, Infrared study of the adsorption of formic acid on clean and Ca-promoted Pd/SiO_2 catalysts, Appl. Catal. A 255 (2003) 181–195.
[51] M.T. Chen, Y.S. Lin, Y.F. Lin, H.P. Lin, J.L. Lin, Dissociative adsorption of HCOOH, CH_3OH and CH_2O on MCM-41, J. Catal. 228 (2004) 259–263.
[52] T. Kecskes, J. Rasko, J. Kiss, FTIR and mass spectrometric study of HCOOH intercalation with supported Rh and Au catalysts, Appl. Catal. A: Gen. 268 (2004) 9–16.

[53] T. Kecskes, R. Nemeth, J. Rasko, J. Kiss, New reaction route of HCOOH catalytic decomposition, Vacuum 80 (2005) 64–68.
[54] R.B. Barros, A.R. Garcia, L.M. Ilharco, The chemistry of formic acid on oxygen modified Ru(0 0 1) surfaces, Surf. Sci. 591 (2005) 142–152.
[55] G. Jacobs, M. Patterson, U.M. Graham, A.C. Crawford, B.H. Davis, Low temperature water gas shift: the link between the catalysis of WGS and formic acid decomposition over Pt/Ceria, Int. J. Energy 30 (2005) 1265–1276.
[56] G. Jacobs, M. Patterson, U.M. Graham, A.C. Crawford, A. Dozier, B.H. Davis, Catalytic links among the water–gas shift, water-assisted formic acid decomposition, and methanol steam reforming reactions over Pt-promoted thoria, J. Catal. 235 (2005) 79–91.
[57] J.F. Lee, C.K. Lee, L.C. Juang, Size effects of exchange cation on the pote structure and surface fractality of montmorillonite, J. Colloid Interface Sci. 217 (1999) 172–176.
[58] M. Önal, Y. Sarıkaya, T. Alemdaroğlu, İ. Bozdoğan, The effect of acid activation on some physicochemical properties of a bentonite, Turk. J. Chem. 26 (2002) 409–416.
[59] T. Alemdaroğlu, G. Akkuş, M. Önal, Y. Sarıkaya, Investigation of the surface acidity of a bentonite modified by acid activation and thermal treatment, Turk. J. Chem. 27 (2003) 675–681.
[60] R.S. Juang, S.H. Lin, F.C. Huang, C.H. Cheng, Structural studies of Na-montmorillonite exchanged with Fe^{2+}, Cr^{3+}, and Ti^{4+} by N_2 adsorption and EXAFS, J. Colloid Interface Sci. 274 (2004) 337–340.
[61] F.C. Huang, J.F. Lee, C.K. Lee, H.P. Chao, Effects of cation exchange on the pore and surface structure and adsorption characteristics of montmorillonite, Colloids Surf. A: Physicochem. Eng. Aspects 239 (2004) 41–47.
[62] C. Mosser, L.J. Michot, F. Villieras, M. Romeo, Migration of cations in copper(II); exchanged montmorillonite and laponite upon heating, Clays Clay Miner. 45 (1997) 789–802.
[63] N. Ozturk, A. Tabak, S. Akgol, A. Denizli, Reversible immobilization of catalase by using a novel bentonite–cysteine microcomposite affinity sorbents, Colloids Surf. A: Physicochem. Eng. Aspects 322 (2008) 148–154.
[64] J.F. Lee, C.K. Lee, L.C. Juang, Size effects of exchange cation on the pore structure and surface fractality of montmorillonite, J. Colloid Interface Sci. 217 (1999) 172–176.
[65] S. Netpradit, P. Thiravetyan, S. Towprayoon, Adsorption of three azo reactive dyes by metal hydroxide sludge: effect of temperature, pH, and electrolytes, J. Colloid Interface Sci. 270 (2004) 255–261.
[66] A. Tabak, E. Eren, B. Afsin, B. Caglar, Determination of adsorptive properties of a Turkish Sepiolite for removal of reactive 15 anionic dye from aqueous solutions, J. Hazard. Mater. 161 (2009) 1087–1094.
[67] E. Tombacz, M. Szekeres, Colloidal behaviour of aqueous montmorillonite suspensions: the specific role of pH in the presence of indifferent electrolytes, Appl. Clay Sci. 27 (2004) 75–94.
[68] A. Tabak, N. Baltas, B. Afsin, M. Emirik, B. Caglar, E. Eren, Adsorption of reactive red 120 from aqueous solutions by cetylpyridinium-bentonite, J. Chem. Technol. Biotechnol. 85 (2010) 1199–1207.
[69] E. Eren, Removal of basic dye by modified Unye bentonite, Turkey, J. Hazard. Mater. 162 (2009) 1355–1363.
[70] T. Higuchi, Mechanism of sustained-action medication, J. Pharm. Sci. 52 (1963) 1145–1149.
[71] J.P. Zheng, L. Luan, H.Y. Wang, L.F. Xi, K.D. Yao, Study on ibuprofen/montmorillonite intercalation composites as drug release system, Appl. Clay Sci. 36 (2007) 297–301.
[72] Z.L. Wang, E.B. Wang, L. Gao, L. Xu, Synthesis and properties of Mg_2Al layered double hydroxides containing 5-fluorouracil, J. Solid State Chem. 178 (2005) 736–741.
[73] T. Heikkila, J. Salonen, J. Tuura, M.S. Hamdy, G. Mul, N. Kumar, T. Salmi, D.Y. Murzin, L. Latinen, A.M. Kaukonen, J. Hirvonen, V.P. Lehto, Mesoporous silica material TUD-1 as a drug delivery system, Int. J. Pharm. 331 (2007) 133–138.